Occurrence and Altitude of the Non-Specular Long-Lived Meteor Trails During Meteor Showers at High Latitudes

A. Kozlovsky[1], R. Lukianova[2,3], and M. Lester[4]

[1]Sodankylä Geophysical Observatory, Sodankylä, Finland.
[2]Space Research Institute, Moscow, Russia.
[3]Saint-Petersburg State University, Russia.
[4]Department of Physics and Astronomy, University of Leicester, Leicester, UK.

Corresponding author: Alexander Kozlovsky (alexander.kozlovsky@oulu.fi)

Key Points:

- Long-lived non-specular echoes from non-field-aligned irregularities constitute 2% of all meteor radar detections
- Long-lived non-specular echoes from non-field-aligned irregularities occur few kilometers higher than other echoes
- Enhanced heights of meteor detections during showers are due to long-lived non-specular echoes from non-field-aligned irregularities

Abstract

Meteoroids entering the Earth's atmosphere produce ionized trails, which are detectable by radio sounding. Cylindrical underdense (and partly overdense) trails form a great majority of meteor echoes received by meteor radars (MR). Additionally, the long-lived non-specular (LLNS) meteor echoes are received from non-field-aligned irregularities of ionization generated along tracks of relatively large meteoroids. The occurrence and height distributions of LLNS are studied using MR observations at Sodankylä Geophysical Observatory (SGO, 67° 22' N, 26° 38' E, Finland) during 2008-2019. Two parameters are analyzed: the percentage and height distribution of LLNS echoes. These LLNS echoes constitute about 2% of all MR detections. However during certain meteor showers (Geminids, Perseids, Quadrantids, Arietids or/and Daytime ζ-Perseids, and Lyrids) the percentage of LLNS echoes is noticeably higher (about 6, 5, 4, 4, and 3%, respectively). Typically, the LLNSs occur ~2 km higher than other echoes (in June-July the height difference is reduced to ~1 km). Due to this elevation, a larger percentage of LLNSs is manifested as an upward shift of the height distribution of meteor trails during meteor showers. Moreover, during Lyrids, η-Aquariids, Perseids, Orionids, and Leonids the LLNS echoes occur noticeably, up to 3-6 km, higher than the echoes from other types of trails. Thus, enhanced heights of meteor detections during major meteor showers (Quadrantids, Lyrids, η-Aquariids, Arietids or/and Daytime ζ-Perseids, Perseids, Orionids, Leonids, and Geminids) are predominantly due to long-lived non-specular echoes from the non-field-aligned irregularities associated with large meteoroids.

Plain Language Summary

Meteoroids entering the Earth's atmosphere produce the ionized trails, which are detectable by radars. Majority of such radar detections are the echoes from cylindrical ionized trails, which occur if the radar beam is perpendicular to the trail, i.e., the reflection is specular. Typically such echoes last less than one second. However, sometimes meteor radars observe unusually long-lived meteor echoes and these echoes are non-specular (LLNS echoes). The LLNS echoes last up to several tens of seconds and show highly variable amplitude of the radar return. The LLNS echoes are received from trails of bright meteors and it is believed that key role in their generation belongs to the aerosol particles arising due to fragmentation and burning of large meteoroids. We found that usually about 2% of all meteor radar detections are LLNS echoes, however during peaks of some meteor showers (Geminids, Perseids, Quadrantids, Arietids or/and Daytime ζ-Perseids, and Lyrids) the percentage is larger, up to 5-6%. On average, the LLNS echoes occur ~2 km higher than other echoes, and even higher (up to 3-6 km) during Lyrids, η-Aquariids, Perseids, Orionids, and Leonids. Thus, these meteor showers are clearly identified in the height distributions of meteor trails.

1 Introduction

Meteoroids are space particles, e.g., the remains of a comet or asteroid. Meteoroids producing visible traces in the Earth's atmosphere are called meteors. The particles of mass larger than 1 μg entering the atmosphere at a speed of few tens km/s, ionize the ambient atmospheric gas and leave cylinder-shaped ionized trails which can be detected by radars (Bronshten, 1983). The majority of ionized meteor trails occur at the heights between 80 and 100 km with a maximum near 90 km. The height distribution depends on the air density and

characteristics of the meteoroids. Annual and year-to-year changes of the meteor height distributions were presented by e.g., Lima et al., 2015; Batubara et al., 2018, who studied data from meteor radars (MR) located at low latitudes to look for effects of solar activity.

Lukianova et al. (2018) investigated annual variations of the height of ionized trails using 9-years (2008-2017) of data from the high-latitude MR located at Sodankylä Geophysical Observatory (SGO, Finland). They analyzed the median height of meteor trails and corresponding upper and lower quartiles and found that meteoroids of some showers produce ionization trails at altitudes noticeably exceeding those of sporadic meteors. Thus, major northern hemisphere meteor showers, namely the Quadrantids, Lyrids, η-Aquariids, Arietids (or/and Daytime ζ-Perseids), Perseids, Orionids, and Geminids were identified as sharp enhancements of the height of ionized trails at peak dates of the showers. It was suggested that the shower meteor trails originate at higher altitudes likely due to higher speed and probably lighter or less dense meteoroids belonging to the showers.

To some degree, the present paper is a continuation of the study of Lukianova at al. (2018). As the next step toward the diagnosis of meteor echoes during meteor showers based on the SGO MR, we investigate in more detail the height distributions and properties of the different types of meteor trails. The SGO MR is a monostatic interferometric meteor radar providing continuous observations based on the specular radio wave scattering from ionized cylinder meteor trails. In addition, a relatively small fraction of the echoes is attributed to long-lived non-specular (LLNS) echoes associated with bright meteors (Chau et al., 2014; Kozlovsky et al., 2018). In the present paper we analyze peculiarities of the individual signals backscattered from the trails and identify these long-lived non-specular (LLNS) meteor echoes. Comparison is made of the occurrence and height distribution of LLNS echoes during the major meteor showers and the non-shower times, when the sporadic meteors dominate. This is the very first study of the statistics of the LLNS echoes.

2 Data

We use data from the meteor radar at Sodankylä Geophysical Observatory (SGO, 67° 22' N, 26° 38' E, Finland) from December 2008 through July 2019. The radar is an all-sky interferometric meteor radar SKiYMET operating at a frequency of 36.9 MHz. Algorithms of the SKiYMET radar signal processing are described in the paper (Hocking et al., 2001). The five-antennae receiving array is arranged as an interferometer, and phase differences in the signals arriving at each of the antennae of the interferometer are used to determine an unambiguous angle of arrival, i.e. allows the determination of meteor echo azimuth and elevation angles. Also, the receiving system determines Doppler velocity of the selected targets.

The top panel in Figure 1 presents the number of meteor trails detected during a day (blue dots). There is an annual variation with a maximum in each summer (more than 15000 meteors per day) and a minimum in each spring (of the order of 4000 detections in a day). On some days, e. g., 13 August and 13 December there are sharp peaks (up to 20000 detections in a day), which are associated with meteor showers. Sharp minima (down to zero) indicate dates of breaks in the radar operation. The count enhancement in September 2009 is due to a radar power upgrade from 7.5 kW to 15 kW.

The inter-pulse frequency of MR transmissions is 2144 KHz, so that the range may be determined with a 70 km ambiguity. To reduce the range ambiguity, the MR data analysis algorithm assumes that meteor trails are preferably at heights between 70 and 110 km, so that about 70% of meteors are located unambiguously. For the height distributions in the present paper we use only unambiguous detections. Following Lukianova et al. (2018), we use only the detections at an elevation angle higher than 30° with a Doppler velocity less than 100 m/s to reject non-meteor targets associated with auroral activity. The number of such detections during a day is shown in top panel in Figure 1 by the red dots. On average, about 50% of all detections were used to study the height distribution of meteor trails.

The bottom panel in Figure 1 presents the time series of daily median (M) and upper (UQ) and lower (LQ) quartiles heights. The black curve shows the smoothed variations obtained by applying a 30-point FFT filter. One can see the quasi-periodic seasonal variations and also short (a few days) enhancements of the meteor height. The latter are usually associated with regular meteor showers, such as the Perseids on 13 August or the Lyrids on 22 April. Such enhancements are the main subject of the present study.

3 Height distribution of meteor trails

Using the height data from the whole 10.5-years period of observations, we have obtained composite histograms representing the averaged height distribution for each day of year. These histogram binned in 1 km height bins are presented in Figure 2 as a color-coded plot. The histograms were normalized by maxima for each day of year. Red curves on the plot show the medians and quartiles of the daily distributions. Numbers from 1 to 8 indicate the meteor showers identified in Lukianova at al. (2018) and listed in Table 1. White curves show the levels of constant atmospheric density (in 10^{-10} g/cm^3) calculated for the SGO site using the Mass-Spectrometer-Incoherent-Scatter NRLMSIS-00 model (Picone et al., 2002).

In Figure 2 one can see that the annual variation of the meteor height distribution agrees, to some extend, with the seasonal variations of the atmospheric density. The other factor affecting seasonal change of meteor trails is the annual variations of radiant of sporadic meteor sources (Kero et al., 2012). These two factors cause a gradual variation of the height, whereas sharp few-days peaks are associated with the meteor showers.

Figure 2 shows that an enhanced percentage of trails is detected above 95 km during certain meteor showers. The most prominent such feature is seen for the Perseids in August (identified as 6). In the following, we first consider in more detail the properties of radar echoes from the Perseids meteor trails observed at altitudes above 95 km and compare them with the detections at 89-91 km, which corresponds to the maximum of the height distribution of meteors.

4 Meteor radar echoes during Perseids

In routine MR operation for each echo accepted as a meteor a short 4 s record of the signals (real and imaginary components) received at five antennas is archived. An example of such a record for a meteor echo detected on 13 August 2018 at 20:42:41 UT is shown in Figure 3a, where the amplitude of the signal received at one of the antennas is presented versus time (zero time corresponds to the time of meteor detection). This is a typical example of an under-

dense meteor trail, and a great majority of the meteor radar echoes are from such type trails, which are produced by relatively small meteoroids. The amplitude of such echoes sharply increases up to a maximum value and then immediately starts to decrease quasi-exponentially. Durations of such echoes detected by the SGO SKiYMET radar are typically less than 0.2 s. The under-dense trails are characterized by a line electron density much less than $2.4 \cdot 10^{14}$ m^{-1} (Bronshten, 1983). More dense trails are classified as intermediate or over-dense. In most cases their duration is up to 1s (for the SGO SKiYMET radar). An example of an over-dense trail is given in Figure 3b. Radio wave reflection (backscattering) from the both under- and over-dense trails is specular, i.e., it occurs when the radar beam is perpendicular to the trail.

In the cases of large meteoroids the meteor radar echoes may have a more complex shape. Examples of such relatively rare detections obtained during Perseids on 13 August 2018 are given in Figure 3 c-e. These echoes were received nearly simultaneously (at 14:15:49 UT) from different ranges (heights) and lasted longer than 3 s exhibiting irregular oscillations of the amplitude. The meteor radar raw data for this event are presented in Figure 4 as a range-time-intensity (RTI) color plot. This plot shows that the meteoroid was descending and moving away from the radar, so that the echoes were received from distances between 182 and 192 km. In the given case the meteor radar detection system identified meteor trails at ranges 186, 188, and 190 km, which correspond to heights 101.7, 100.9, and 98.9 km, respectively (indicated on the right in Figure 4 and presented in Figure 3 c-e). At the last ranges the radar reflections lasted about 40 s. Such meteor radar detections are classified as long-lived non-specular echoes (Chau et al., 2014) and in many cases they were observed at heights between 95 and 110 km (Kozlovsky et al., 2018).

We now investigate whether the presence of the long-lived non-specular (LLNS) echoes can be responsible for the enhanced altitude of meteor echoes during Perseids. During the whole day 13 August 2018 there were 1315 meteor echoes obtained from 95-105 km and 1005 detections at 89-91 km. Their 4-s power records are presented in Figure 5 a and b as color-coded plots as functions of the record duration time (horizontal axes) and time of detection (vertical axes). The LLNS echoes are manifested as horizontal lines continuing from 0 to 3 s. It may be noticed by eye that the relative number of the LLNS echoes is larger above 95 km (Figure 5a), compared to heights between 89 and 91 km (Figure 5b).

We developed a simple algorithm to separate the LLNS echoes. We have analyzed the 4-s amplitude records and compared the median amplitude between 1.0 and 0.5 s prior to the onset of a meteor detection and the median amplitude between 0.5 and 3.0 s after the onset of a meteor detection (i.e. the zero time). If the second was 1.5 times larger than the first one, the detection was identified as LLNS. The threshold of 1.5 was selected empirically such as the algorithm distinguishes correctly LLNS from others trails.

Figure 6 presents the same data as Figure 5, although the data were re-ordered in such a way that the identified LLNS detections are placed in the bottom of each plot and other detections are above. One can see that between 95 and 105 km 203 of 1315 detections (i.e., 15 %) were LLNS, whereas at 89-91 km they were only 3 %. This indicates a role of LLNS echoes in the height distribution of Perseids. Figure 6 also shows that the algorithm identifies correctly majority of LLNS trails. In the following we apply this method to the whole database of the SGO meteor radar for a more rigorous analysis.

5 Statistics of the long-lived trails

Routinely, the 4-s records of the signals received at five antennas are to be archived for all detections. However in 2010 and during April 2013 – March 2014 the data were lost, so that the 4-s records exist only for about 80 % of all detections. All these data were analyzed to separate LLNS echoes and other trails. Altogether, more than $9 \cdot 10^6$ echoes were analyzed and about $2 \cdot 10^5$ of them were identified as LLNS.

Characteristics of the detections averaged over a day of the year are presented in Figure 7. The top panel (Figure 7a) shows the percentage of the LLNS detections as a function of the day of year. Numbers 1-8 indicate the meteor showers distinguished in the height distributions of meteor echoes (Lukianova et al., 2018) and presented in Table 1. On average, about 2 % of the detections are LLNS, but during some showers, notably the Geminids, Perseids, Quadrantids, Arietids/Daytime ζ-Perseids, and Lyrids, the percentage is noticeably higher by up to 6, 5, 4, 4, and 3%, respectively.

Figure 7b shows medians and quartiles of the height distributions of the LLNS (red) and the other echoes when LLNS are excluded (blue). The formers are typically detected ~2 km higher than the latter (except June-July when the height difference is about 1 km). During some showers, namely, the Lyrids (3), η-Aquariids (4), Perseids (6), and Orionids (7), the upper quartile of LLNS echoes is up to 5-6 km higher than that of other trails. A remarkable peak in the upper quartile of LLNS echoes is seen on 19 November. This date corresponds to the peak of Leonids meteor shower, although the median and quartiles of all echoes on this day (Figure 2) show a very small enhancement so that this shower was not identified in (Lukianova et al., 2018). Nevertheless, because of the prominent peak in the upper quartile of LLNS echoes we decided to add the Leonids shower to Table 1.

Comparing Figure 7b with Figure 2, one can notice that the signatures of meteor showers presented in the height distributions (median and quartiles) of all echoes (Figure 2) are clearly less prominent in the heights of echoes when LLNS echoes are excluded (blue curves in Figure 7b). Hence, enhanced heights of meteor detections during major meteor showers are essentially due to long-lived non-specular echoes.

6 Discussion: LLNS echoes in association with meteor showers

6.1 Properties and possible mechanisms for the LLNS detections

Cases of long-lived non-specular meteor echoes observed at high latitudes have been reported in several papers (Kelley et al., 1998; Röttger, 2000; Close et al., 2011; Chau et al., 2014). Using data from collocated optical, radar, and ionosonde observations at SGO Kozlovsky et al. (2018) studied bright meteors creating dense ionization trails with an initial line electron density between 10^{14} and 10^{16} m^{-1}. They have shown that in many cases meters-scale irregularities of electron density are formed along the tracks of such bright meteors, so that the meteor radar detects non-specular reflections from them. At low latitudes non-specular meteor echoes can originate from magnetic-field-aligned irregularities of electron density (e.g., Oppenheim et al., 2003; Dyrud et al., 2011), but it is impossible at the high-latitude SGO site where the magnetic field lines are close to the vertical. Hence, we deal with long-lived non-specular meteor echoes from non-field-aligned irregularities of electron density.

To explain non-specular long-lived echoes from meteor trails at high latitudes, Chau et al. (2014) suggested that: "…echoes could be qualitatively explained by the presence of charged dust forming from the meteoric material immersed in a turbulent flow. This can lead to a high Schmidt number plasma that can sustain meter-scale turbulence just as it does for the polar mesospheric summer echoes. These rare events require relatively large meteoroids." Thus, a mechanism of LLNS echoes may be analogous to the polar mesosphere summer echoes (PMSE) provided that meteor smoke particles play the role of ice particles. The meter-scale structures of electron density may be formed due to the neutral turbulence as Chau et al. (2014) suggested. An alternative mechanism may be the instability, which is due to the charged meteor smoke particles moving downwards under the influence of gravity, so that they move relatively to the background plasma. This relative motion leads to the dissipative instability, a mechanism which is analogous to that of the resistive beam-plasma instability. As a result, meter scale irregularities (electrostatic waves) are generated. Trakhtengerts (1994) suggested this instability for explaining PMSE, and later Kozlovsky et al. (2017) used this model to explain meteor radar echoes from the mesospheric plasma irregularities caused by the missile destruction in December 2009. This instability requires relatively large (of the order of 40 nm) aerosol particles. Irrespective of the particular mechanism, turbulence or instability, we believe that the aerosol particles along trajectories of large meteors are the main factor responsible for LLNS echoes. These particles presumably occur due to fragmentation and burning of large meteoroids. Further discussion of the mechanisms of LLNS echoes is out of scope of the present paper where we pay the main attention to statistics of the occurrence and height of LLNS echoes.

6.2 LLNS echoes in association with meteor showers

Analyzing the 10.5-years statistics of LLNS detections by the high-latitude MR we have found that such events are not too rare. Indeed, LLNS make typically about 2% of all meteor radar detections, i.e., about 200 echoes every day, whereas during the Geminids or Perseids number of such detections may be up to 5-6 %, i.e., up to 1000 in a day.

Table 1 summarizes the data of percentage of LLNS echoes during meteor showers and also gives the height differences between LLNS and other echoes (ΔLQ, ΔLQ, and ΔLQ). As was shown in Figure 7a, typically about 2 % of the detections are LLNS, although during certain showers the percentage is noticeably larger, and these showers (Geminids, Perseids, Quadrantids, Arietids/Daytime ζ-Perseids, and Lyrids) are indicated by letter "P" in "Type" column in Table 1. Letter "H" indicates the showers during which the height difference between LLNS and other echoes stands out. Such showers are the Lyrids, η-Aquariids, Perseids, Orionids, and Leonids. For them, LLNS echoes are detected 3-6 km higher than other meteor echoes. Apart from these showers the height difference is about 2 km, except in June and July when the difference is smaller (about 1 km) obviously due to lower temperature and, respectively, larger air density in the polar summer mesosphere. In Table 1 we notice that the unknown shower on January 28-29 is manifested neither in the height difference nor in the percentage of LLNS trails. We believe it may be associated with the Antihelion sporadic meteors source rather than a specific meteor stream. Due to this, the event on January 28-29 is excluded from further consideration.

Now we focus on the meteor showers which are classified as P, PH, or H in Table 1. For them, three different reasons may underlie the increased height of meteor trails. First, the height elevation may be due to a larger percentage of LLNS trails (P). The second possibility is the

occurrence of LLNS trails at higher altitudes (H). Finally, a combination of the two reasons may be in effect.

In the characteristics of the showers listed in Table 1, we notice some regularity. The three last columns present the following parameter of the meteor streams: geocentric velocity V_G, right ascension *RA*, and declination *D* according to Kronk (2014). Looking at the data, we have noticed some correspondence between the type of meteor shower and velocity of the meteoroids entering the atmosphere. Namely, the P-type shower meteoroids (Quadrantids, Arietids or/and Daytime ζ-Perseids, and Geminids) have the lowest velocity, 29-39 m/s, for the PH-type (Lyrids and Perseids) the velocity is higher, 47-61 km/s, and the highest velocity, 65-67 km/s, is during the H-type showers (Orionids, and Leonids).

It is well established that the meteoroids entering the atmosphere at higher speed ablate in less dense air, hence, at a higher altitude (Popova et al., 2019). This agrees with the result of the present paper that showers of larger speed meteors (47-67 km/s) are manifested as enhanced altitude of LLNS trails (H and PH types). At the same time, our observations reveal that lower-speed (29-39 km/s) meteoroids produce enhanced (4-6%) number of LLNS trails. This may be consistent with the fragmentation which reduce the meteor velocity and enhance the clouds of dust and aerosol particles. As pointed out by Popova et al. (2019), during the entry of a meteoroid the fragmentation is more important than both the deceleration and ablation. A meteoroid is disrupted into a swarm of smaller bodies, which continue their flight as a single mass with increasing cross-section and decreasing velocity. Less dense (crumbly, porous) meteoroids are the most suitable for fragmentation and filling the volume between larger particles by the evaporated material. Density and porosity depend on the meteor composition and structure, the latter shows a wide scatter but usually is about a few percent (e.g. ordinary chondrite has on average a porosity of 8-10% (Macke et al, 2010)). Smaller particles with lower velocity have a higher chance of longer survival. This can possibly explain a larger number of LLNS echoes from the lower-speed meteors.

During the Geminids peak (14 December), the height of LLNS echoes is almost the same as that of the other meteor trails. Because of this, the height enhancement during Geminids is not so prominent in spite of the highest percentage (6.4%) of LLNS trails. The Geminid shower is observed between 6 and 19 December (Kronk, 2014), which coincide with the clear drop of the UQ and M heights of LLNS echoes down to these of the other echoes. This is different from other meteor showers and even sporadic meteor sources, for which the height of LLNS echoes is higher than that of other (under- and over- dense trails). This may indicate specific properties (mass, density, chemical composition) of the Geminids meteoroids, which agrees with (Kozlovsky et al., 2016) who analyzed the height-lifetime distributions of meteor trails and came to conclusion on specific properties of Geminids.

7 Summary

We present statistics of occurrence and height distributions of long-lived non-specular (LLNS) meteor echoes observed during 10.5 years at high latitudes. Such echoes are received from non-field-aligned irregularities generated along tracksof relatively large meteoroids. Aerosol particles arising due to fragmentation and burning of the meteoroids play a key role in

the generation of the irregularities. The echoes last up to several tens of seconds exhibiting highly variable amplitude of the radar return.

The LLNS meteor echoes constitute about 2% of all meteor radar detections, while during some showers (Geminids, Perseids, Quadrantids, Arietids or/and Daytime ζ-Perseids, and Lyrids) the percentage of LLNS echoes is noticeably higher (of the order of 6, 5, 4, 4, and 3%, respectively).

The LLNS meteor echoes typically occur ~2 km higher than other echoes (except June-July when the height difference is ~1 km). Because of that, la arger percentage of LLNS during some meteor showers is manifested as an upward shift of the height distribution of meteor trails. Moreover, during some showers (Lyrids, η-Aquariids, Perseids, Orionids, and Leonids) the LLNS echoes occur noticeably (up to 3-6 km) higher than other trails.

Thus, one of two factors, the enhanced percentage of LLNS trails or the enhanced height of LLNS trails, or a combination of both lead to enhanced heights of meteor detections during some meteor showers. The first factor is essential for slower speed meteor stream (29-39 m/s, the Quadrantids, Arietids or/and Daytime ζ-Perseids, and Geminids), the second one is important for higher speed streams (65-67 km/s, the Orionids, and Leonids), while both factors play role for the medium speed streams (47-61 km/s, the Lyrids and Perseids).

To summarize, the most important finding of the present study is that enhanced heights of meteor detections during major meteor showers (Quadrantids, Lyrids, η-Aquariids, Arietids or/and Daytime ζ-Perseids, Perseids, Orionids, Leonids, and Geminids) are predominantly due to long-lived non-specular echoes from the non-field-aligned irregularities associated with large meteoroids.

Acknowledgments

The meteor radar data were collected at SGO (http://www.sgo.fi/). RL acknowledges support from the Academy of Finland via grant 310348. ML acknowledges support from Science and Technology Facilities Council (STFC) via grant ST/S000429/1. The authors acknowledge discussions within the International Space Science Institute (ISSI) Team 410 on New Features in the Meteor Radar Observations and Applications for Space Research.

References

Bronshten, V. A. (1983). *Physics of Meteoric Phenomena*, (356 pp.). Dordrecht, Holland: Kluwer.

Chau, J. L., Strelnikova, I., Schult, C., Oppenheim, M. M., Kelley, M. C., Stober, G., & Singer, W. (2014), Nonspecular meteor trails from non-field-aligned irregularities: Can they be explained by presence of charged meteor dust? *Geophys. Res. Lett.*, 41, 3336–3343, doi:10.1002/2014GL059922.

Close, S., M. Kelley, L. Vertatschitsch, P. Colestock, M. Oppenheim, & J. Yee (2011), Polarization and scattering of a long-duration meteor trail, *J. Geophys. Res.*, 116, A01309, doi:10.1029/2010JA015968.

Dyrud, L. P., Urbina, J., Fentzke, J. T., Hibbit, E., & Hinrichs, J. (2011), Global variation of meteor trail plasma turbulence, *Ann. Geophys*., 29, 2277-2286.

Hocking, W.K., Fuller, B., & Vandepeer, B. (2001), Real-time determination of meteor-related parameters utilizing modern digital technology. *Journal of Atmospheric and Solar-Terrestrial Physics*, 63, 155-169.

Kelley, M. C., C. Alcala, & J. Y. N. Cho (1998), Detection of a meteor contrail and meteoric dust in the Earth's upper mesosphere, *Journal of Atmospheric and Solar-Terrestrial Physics*, 60, 359–369, doi:10.1016/S1364-6826(97)00113-2.

Kero, J., Szasz, C., Nakamura, T., Meisel, D. D., Ueda, M., Fujiwara, Y., et al. (2012). The 2009–2010 MU radar head echo observation programme for sporadic and shower meteors: Radiant densities and diurnal rates. *Monthly Notices of the Royal Astronomical Society*, 425(1), 135–146. https://doi.org/10.1111/j.1365-2966.2012.21407.x

Kozlovsky, A., Shalimov, S., Kero, J., Raita, T., & Lester, M. (2018), Multi-instrumental observations of nonunderdense meteor trails, *J. Geophys. Res. Space Physics*, 123, 5974–5989, https://doi.org/10.1029/2018JA025405.

Kozlovsky, A., S. Shalimov, & M. Lester (2017), Mesospheric plasma irregularities caused by the missile destruction on 9 December 2009, *J. Geophys. Res. Space Physics*, 122, 6696–6707, doi:10.1002/2017JA024300.

Kozlovsky, A., R. Lukianova, S. Shalimov, & M. Lester (2016), Mesospheric temperature estimation from meteor decay times during Geminids meteor shower, *J. Geophys. Res. Space Physics*, 121, 1669–1679, doi:10.1002/2015JA022222.

Kronk, G. W. (2014). *Meteor showers: An annotated catalog* (361 pp.). New York: Springer. https://doi.org/10.1007/978-1-4614-7897-3

Lima, L. M., Araújo, L. R., Alves, E. O., Batista, P. P., & Clemesha, B. R. (2015). Variations in meteor heights at 22.7°S during solar cycle 23. *Journal of Atmospheric and Solar-Terrestrial Physics*, 133, 139–144. https://doi.org/10.1016/j.jastp.2015.08.015.

Lukianova, R., Kozlovsky, A., and Lester, M. (2018), Recognition of Meteor Showers From the Heights of Ionization Trails, *J. Geophys. Res. Space Physics*, 123, 7067–7076, https://doi.org/10.1029/2018JA025706.

Macke, R. J., Consolmagno, G. J., Britt, D. T., & Hutson, M. L. (2010). Enstatite chondrite density, magnetic susceptibility and porosity. *Meteoritics & Planetary Science*, 45, 1513-1526.

Oppenheim, M. M., Dyrud, L. P., & Ray, L. (2003), Plasma instabilities in meteor trails: Linear theory, *J. Geophys. Res*., 108(A2), 1063, doi:10.1029/2002JA009548.

Picone, J., Hedin, A., Drob, D., & Aikin, A. (2002), NRLMSISE-00 empirical model of the atmosphere: Statistical comparisons and scientific issues, *J. Geophys. Res.*, 107(A12), 1468, doi:10.1029/2002JA009430.

Popova O., Borovichka J., Campbell-Brown M., (2019), Modelling the entry of meteoroids. In: G. Ryabova, D. Asher, M. Campell-Brown (Eds), *Meteoroids, Sources of Meteor on Earth and Beyond.* Cambrridge University Press, pp. 9-36.

Röttger, J. (2000), Radar investigations of the mesosphere, stratosphere and the troposphere in Svalbard, *Adv. Polar Upper Atmos. Res*., 14, 202–220.

Trakhtengerts, V. Y. (1994), Generation mechanism of polar mesosphere summer echoes, *J. Geophys. Res.*, 99(D10), 21083–21088, doi:10.1029/93JD03280.

Figure 1. (*top*) Daily number of meteor echoes detected by the meteor radar (blue) and number of the echoes used in the study: unambiguous detections at elevation higher than 30° with the Doppler velocity less than 100 m/s (red). Count enhancement in September 2009 is due to the radar power upgrade from 7.5 kW to 15 kW. (*bottom*) Daily median (M) and upper (Uq) and lower (Lq) heights of meteor detection. The black line depicts a smoothed curve.

Figure 2. The 10.5-years composite histograms representing averaged height distribution for each day of year (color-coded, normalized by maxima for the day of year). Red curves show median and upper and lower quartiles of the distribution. The numbers in the red circles correspond to the first column of Table 1. The white curves show the levels of constant atmospheric density (in 10^{-10} g/cm^{-3}) calculated for the Sodankylä Geophysical Observatory site using the NRLMSISE-00 model.

Figure 3. Amplitude of the signals received at one of the five MR antennas versus time (zero time approximately corresponds to the time of meteor detection): (a) typical example of underdense trail; (b) an overdense trail; (c-e) long-lived non-specular echoes.

Figure 4. The range-time-intensity (RTI) color plot showing meteor radar raw data for the event of long-lived non-specular echoes.

Figure 5. Color-coded plots showing power of the signals received at one MR antenna during 13 August 2018 as functions of the record duration time (horizontal axes) and time of detection (vertical axes): (a) echoes obtained from 95-105 km; (b) echoes obtained from 89-91 km.

Figure 6. The same data as Figure 5, however the data were re-ordered in such a way that the identified LLNS detections are placed in bottom of the plots and other detections are above.

Figure 7. Characteristics of the detections averaged over a day of the year: (a) percentage of the LLNS detections as a function of the day of year; (b) medians and quartiles of the height distributions of the LLNS (red) and others (blue) echoes. Numbers 1-8 indicate the meteor showers presented in Table 1.

434 **Table 1.** Characteristics of the Meteor Showers: Ordinal Number Since the Beginning of the
435 Year, Date of the Maximal Height Peak, Name of the Shower, Percent of NSLL Trails, Height
436 Differences of NSLL and Other Trails for Quartiles and Medians, Type of the Shower (See
437 Section 6.2), Geocentric Velocity VG, Right Ascension RA, Declination D.
438
439

#	Date of h max	Showers	%	ΔLQ km	ΔM km	ΔUQ km	Type	V_G km/s	RA deg.	D deg.
1	Jan 3	Quadrantids	4.4	3	2	1	P -	29	230	+49
2	Jan 28-29	Unknown	<2	2	2	2	- -			
3	Apr 22	Lyrids	2.5	5	5	5	P H	47	272	+33
4	May 6	η-Aquariids	2.0	3	3	5	- H	65	337	−1
5	Jun 9	Arietids Daytime ζ-Perseids	4.0	1.5	1	0.5	P -	39 26	45 63	+24 +26
6	Aug 12	Perseids	5.2	3	4	4	P H	61	48	+57
7	Oct 23	Orionids	<2	3	4	6	- H	65	96	+16
	Nov 19	Leonids	<2	3	3	4	- H	67	154	+22
8	Dec 13	Geminids	6.4	2	1	0	P -	35	113	+32

440

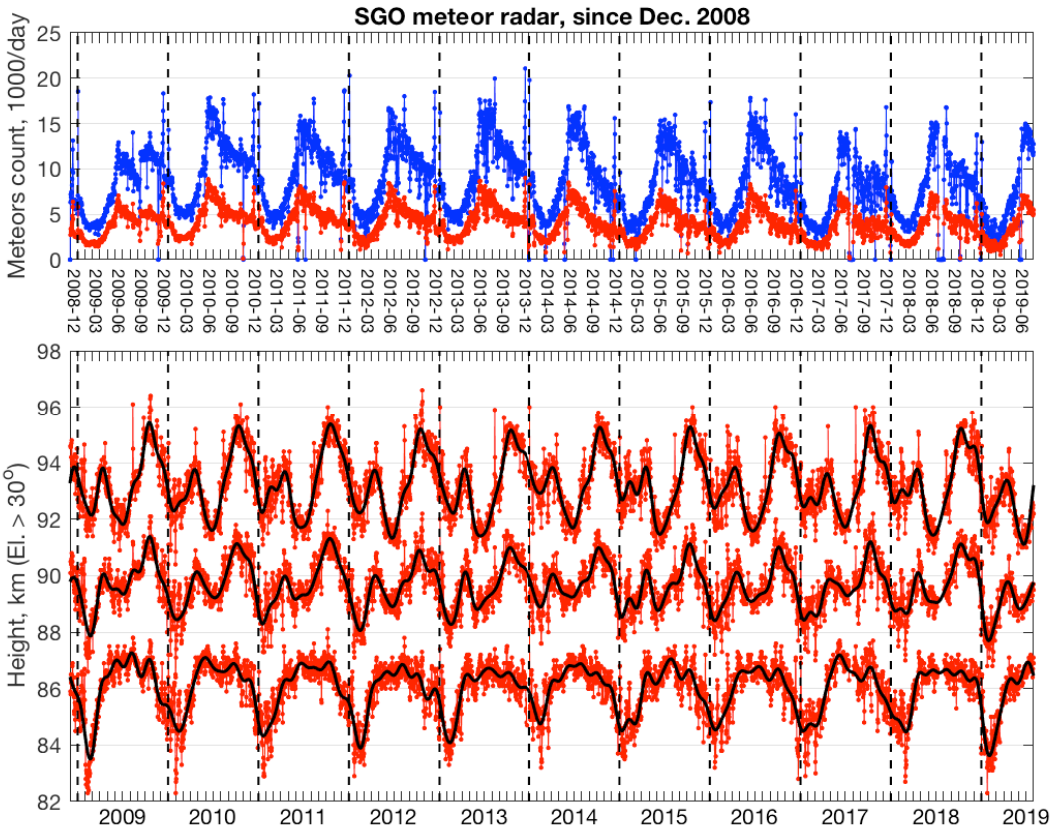

Figure 1. (*top*) Daily number of meteor echoes detected by the meteor radar (blue) and number of the echoes used in the study: unambiguous detections at elevation higher than 30° with the Doppler velocity less than 100 m/s (red). Count enhancement in September 2009 is due to the radar power upgrade from 7.5 kW to 15 kW. (*bottom*) Daily median (M) and upper (Uq) and lower (Lq) heights of meteor detection. The black line depicts a smoothed curve.

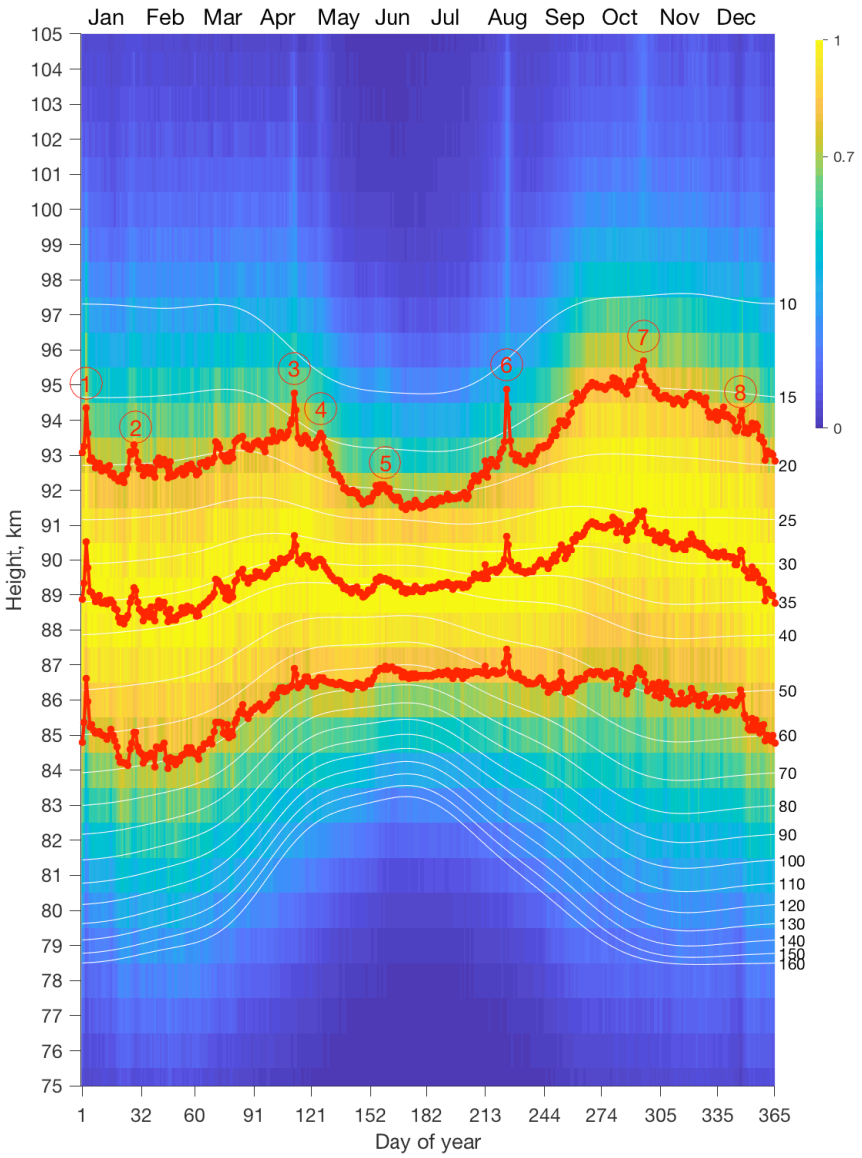

Figure 2. The 10.5-years composite histograms representing averaged height distribution for each day of year (color-coded, normalized by maxima for the day of year). Red curves show median and upper and lower quartiles of the distribution. The numbers in the red circles correspond to the first column of Table 1. The white curves show the levels of constant atmospheric density (in 10^{-10} g/cm^{-3}) calculated for the Sodankylä Geophysical Observatory site using the NRLMSISE-00 model.

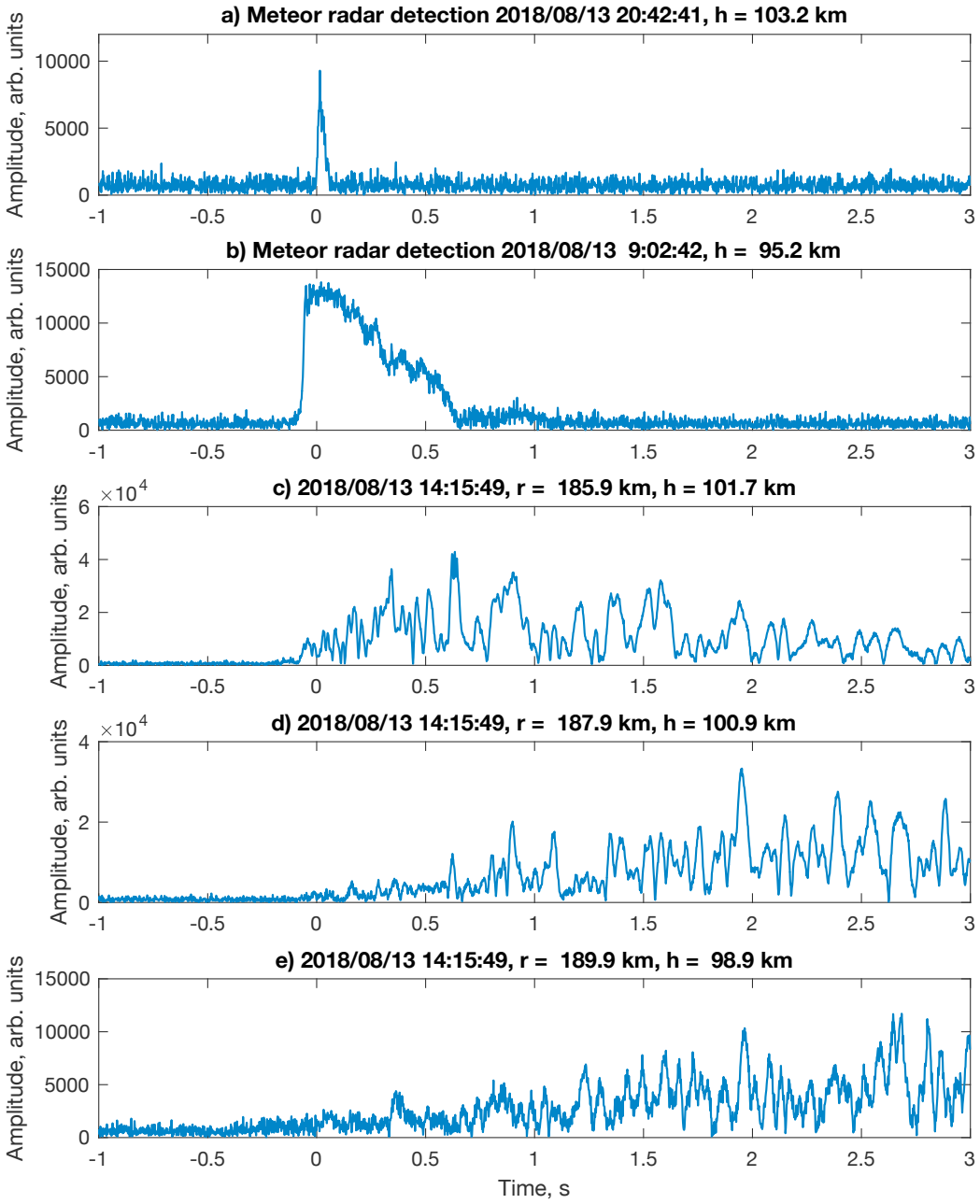

Figure 3. Amplitude of the signals received at one of the five MR antennas versus time (zero time approximately corresponds to the time of meteor detection): (**a**) typical example of underdense trail; (**b**) an overdense trail; (**c-e**) long-lived non-specular echoes.

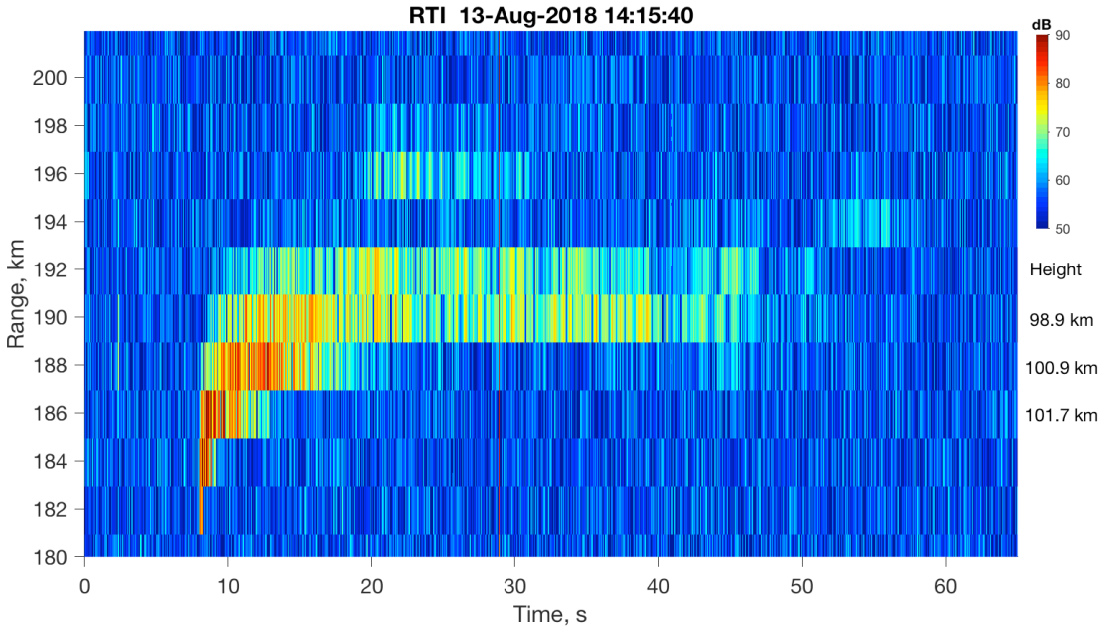

Figure 4. The range-time-intensity (RTI) color plot showing meteor radar raw data for the event of long-lived non-specular echoes.

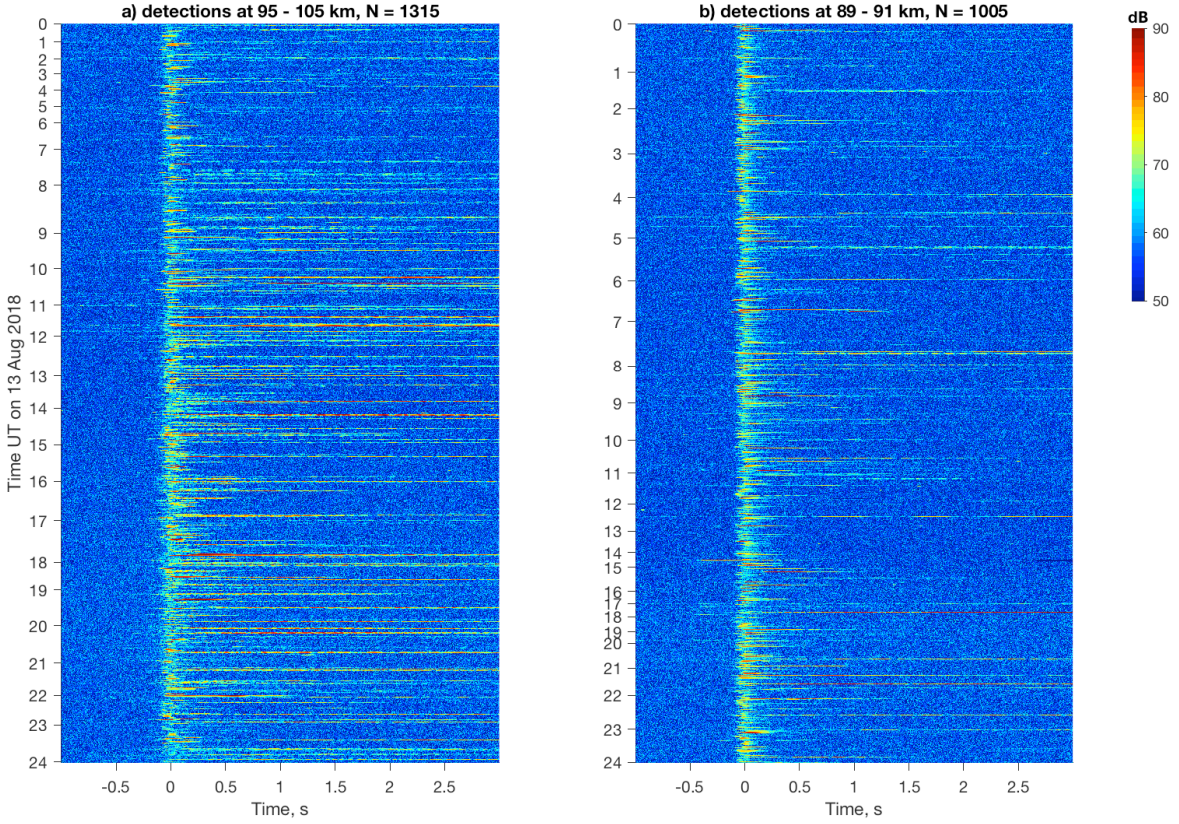

Figure 5. Color-coded plots showing power of the signals received at one MR antenna during 13 August 2018 as functions of the record duration time (horizontal axes) and time of detection (vertical axes): (**a**) echoes obtained from 95-105 km; (**b**) echoes obtained from 89-91 km.

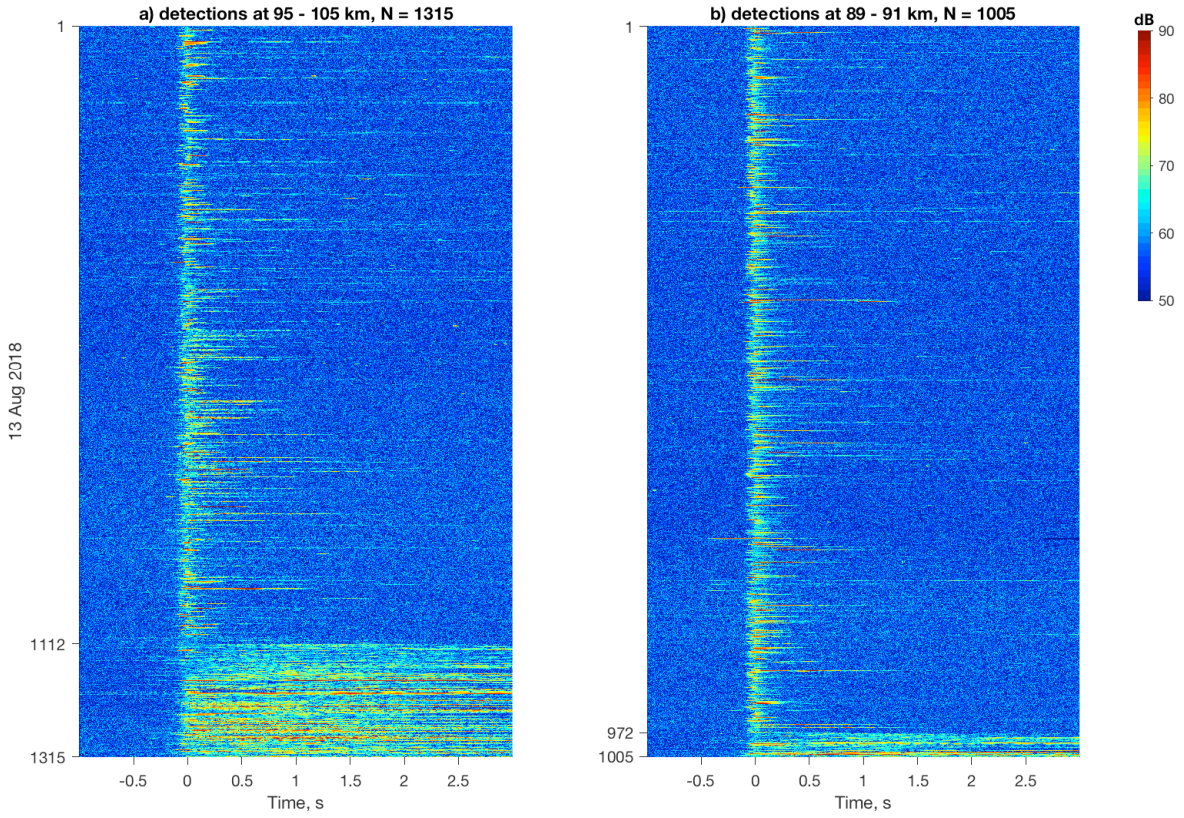

Figure 6. The same data as Figure 5, however the data were re-ordered in such a way that the identified LLNS detections are placed in bottom of the plots and other detections are above.

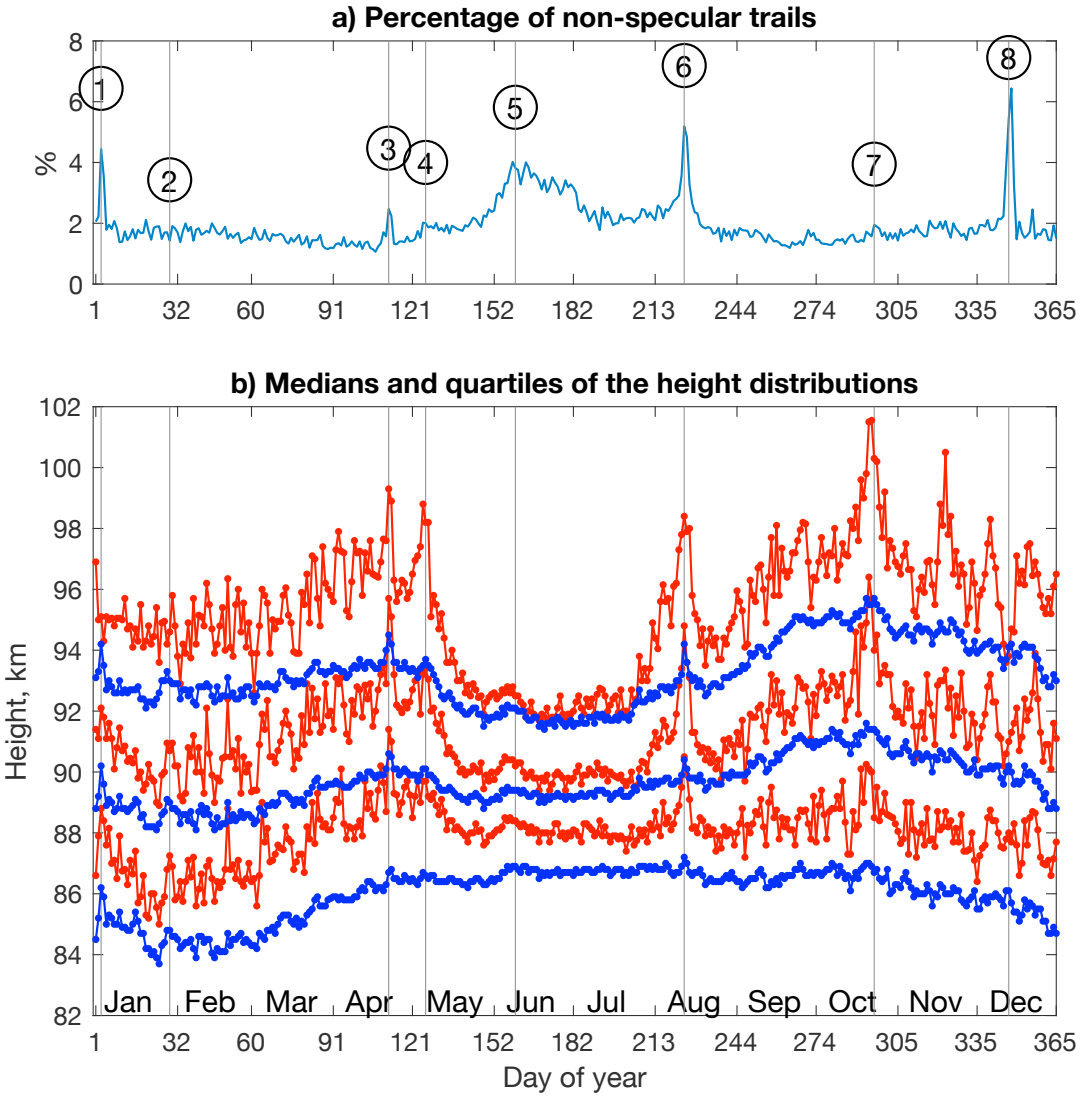

Figure 7. Characteristics of the detections averaged over a day of the year: (**a**) percentage of the LLNS detections as a function of the day of year; (**b**) medians and quartiles of the height distributions of the LLNS (red) and others (blue) echoes. Numbers 1-8 indicate the meteor showers presented in Table 1.